Magnetic interface coupling between Co and binary Fe_xMn_{100-x} alloys in the ultrathin film limit

J. Seifert, T. Bernhard, M. Gruyters,* and H. Winter
Institut für Physik, Humboldt-Universität zu Berlin, Newtonstrasse 15, 12489 Berlin, Germany
(Received 14 May 2007; revised manuscript received 1 August 2007; published 6 December 2007)

The structural and magnetic properties of Fe_xMn_{100-x} single and Co/Fe_xMn_{100-x} bilayers have been investigated by grazing ion scattering, Auger electron spectroscopy, low energy electron diffraction, and magneto-optical Kerr effect. The increase in coercivity of the Co hysteresis loops is used as a measure of the magnetic interface coupling in the bilayers. For FeMn films of 4 ML (monolayers), the onset of coupling is still detectable for temperatures below 160 K. The strength of the coupling rapidly increases with increasing FeMn thickness. At 8 ML FeMn, appreciable interaction is observed at room temperature. For further increasing FeMn thickness, the Co films reveal a significant difference in the behavior of surface and bulk magnetizations.

DOI: 10.1103/PhysRevB.76.224405 PACS number(s): 75.70.−i, 75.30.Gw, 75.60.Jk, 79.20.Rf

I. INTRODUCTION

The study of magnetic 3*d*-transition metal alloy films is of interest in scientific research and technology. In the past two decades, a great variety of applications have been developed in sensor and storage media using these types of materials,[1,2] where magnetoresistive and magnetic anisotropy effects play a decisive role. One of the basic principles is the combination of at least two ferromagnetic layers which are separated by a nonmagnetic spacer.[3] The magnetization of one of the layers is usually free to switch with an externally imposed field, while the magnetization of the other layer is pinned in a certain direction by a neighboring antiferromagnetic layer. The pinning results from interface coupling in the ferromagnetic/antiferromagnetic (FM/AFM) bilayer.[4] Mn-based binary and ternary alloys are frequently used as pinning layers because they possess adequate antiferromagnetic properties over a wide range of concentrations and compositions.

Fe_xMn_{100-x} alloys have been studied for several decades.[5–7] In the bulk, the structural and magnetic properties are usually classified into three concentration regimes with $x \leqslant 30$ (I), $30 \leqslant x \leqslant 70$ (II), and $x \geqslant 80$ (III). On the Mn-rich (regime I) and the Fe-rich (regime III) side, bcc-like structures are most stable at room temperature.[7] Fcc-like structures may be obtained at high temperatures[7] by pseudomorphic growth of thin films on appropriate substrates[8] or by addition of small amounts of a third element such as Cu.[6] In the intermediate range of concentrations (regime II), the fcc structure is the most stable one. Bulk γ-Fe_xMn_{100-x} shows antiferromagnetic order with Néel temperatures T_N between 350 and 520 K.

In order to study the exchange coupling between ferromagnets and antiferromagnets,[4] γ-FeMn films are predominantly used in combination with ferromagnetic 3*d*-transition metal films. Pure metals such as Co or metal alloys such as $Ni_{80}Fe_{20}$ are preferred due to their stable fcc structure and their small lattice mismatch with respect to γ-FeMn. In magnetic hysteresis loops, the interface coupling manifests itself in an enhanced loop half-width H_C and a shift from zero field H_E. The loop shift, termed "exchange bias," can be induced by cooling the FM/AFM bilayer through the Néel temperature in an external field or by applying an external field during film deposition. The observable strength of the effect, i.e., the magnitude of the loop shift H_E and the increase in coercivity H_C, crucially depends on the absolute and relative thicknesses of both films.

Two different methods have been employed for the preparation of FM/FeMn bilayers: sputter deposition and molecular beam epitaxy (MBE). Studies based on the sputtering technique are usually limited to films of several ten monolayers (ML).[9–12] Recent works on MBE-grown bilayers on Cu(001) single crystals concentrate on the ultrathin film regime with a total thickness below 20–30 ML.[13–16] Similar to the heteroepitaxial model systems for two-dimensional film growth, Fe/Cu(001) (Refs. 17–19) and Co/Cu(001) (Refs. 20 and 21), layer-by-layer growth has been established for Fe_xMn_{100-x} on Cu(001) at room temperature.[13,15] A pseudomorphic behavior with fcc-like structures has been found in all three cases. $Fe_{50}Mn_{50}$ films have been reported to enter the antiferromagnetic state above approximately 10 ML at room temperature for both $Co/Fe_{50}Mn_{50}/Cu(001)$ (Ref. 14) and $Fe_{50}Mn_{50}/Co/Cu(001)$ (Refs. 13 and 16) systems. Criteria for the transition are characteristic changes in the magnetic behavior of the exchange-coupled Co film such as an increase in coercivity of the hysteresis loop.

In this paper, we address the structural and magnetic properties of MBE-grown Fe_xMn_{100-x} single and Co/Fe_xMn_{100-x} bilayers on a Cu(001) substrate over the whole concentration range. The Fe_xMn_{100-x} layer thickness is systematically varied in the ultrathin film limit with total thicknesses below 20–25 ML for $x \approx 50$.

II. EXPERIMENT

The experiments were performed in an ultrahigh vacuum setup at a base pressure in the 10^{-11} mbar range, attached via differential pumping stages to the beam line of a small electrostatic ion accelerator. The Cu(001) single crystal surface was prepared by cycles of grazing sputtering with 25 keV Ar^+ ions and subsequent annealing at 770 K for about 20 min. Mn, Fe, and Co were deposited by molecular beam epitaxy at rates of 0.5–1 ML/min, with the substrate held at room temperature. Fe_xMn_{100-x} films were obtained by simultaneous evaporation of Mn and Fe from two different electron beam evaporators. The alloy compositions were pre-

pared by adjusting the individual deposition rates. The chemical composition and the crystalline structure of the substrate and the films were investigated by Auger electron spectroscopy and low energy electron diffraction (LEED), respectively.

For the application of various grazing ion scattering techniques, well collimated beams of H and He atoms or ions with energies of some 10 keV were directed on the crystal surface at polar angles of incidence Φ_{in} of 1.0°–1.5° with respect to the surface plane. In order to study film growth, the intensity of specularly reflected 25 keV He projectiles was recorded as a function of deposition time.

For ion beam triangulation (IBT),[19,22] the ion-induced emission of electrons was monitored as a function of azimuthal angle of incidence Θ for grazing scattering of 29 keV protons. The electrons were detected by a surface barrier detector [23](SBD) positioned at a distance of about 0.1 m from the target surface. The SBD is biased to a high voltage of about 20 kV, where the pulse height is proportional to the number of emitted electrons per scattering event, and allows one to study electron number spectra.[24] A detection scheme is used with a discriminator level of the SBD set to a pulse height interval equivalent to low electron numbers from about two to four electrons. This signal is normalized to the overall detector counts. Since penetration into the bulk for scattering along axial channels results in a considerable enhancement of the electron yield, arrangements of atomic strings (i.e., low-index crystalline directions) in the surface are identified by the reduction of the signal for events related to the emission of low electron numbers. For the separation of low electron numbers, the information depth of the technique thus amounts to the topmost surface layer. A more detailed description of this variant of the IBT method is given elsewhere.[25]

For the scattering experiments on electron capture (EC) into excited levels of He atoms, the emitted polarized fluorescence light of the $2s\ ^3S-3p\ ^3P$ transition at $\lambda=388.9$ nm was detected through a quartz window by means of a quarter-wave retarder plate, a narrow bandwidth interference filter, a linear polarizer, and a cooled photomultiplier.[26–28] The concepts and analysis of experiments on polarized light emission after electron capture are described in detail in Refs. 26–28. In brief, the spin polarization P_s of captured electrons can be deduced from the circular polarization of the fluorescence light described by the Stokes parameter $S/I=[I(\sigma^-)-I(\sigma^+)]/[I(\sigma^-)+I(\sigma^+)]$, where $I(\sigma^-)$ and $I(\sigma^+)$ are the intensities of light with negative and positive helicities, σ^- and σ^+, respectively.[29] P_s is obtained from measurements of the Stokes parameter S/I with reversed settings of the magnetization $(\uparrow,\downarrow)$, where $\Delta S/I=S/I(\uparrow)-S/I(\downarrow)$.[27] For the $2s\ ^3S-3p\ ^3P$ transition of He, P_s is derived from calculations on quantum mechanical coupling of angular momentum and on the radiative decay of the $3p\ ^3P$ term. P_s and $\Delta S/I$ are related to the long-range magnetic order (magnetization M_{FM}) of the sample surface,[30,31] although a quantitative relation has not been established so far. The probing depth of electron capture amounts to the topmost atomic layer at the surface ($\lambda \rightarrow 0$ ML).[30]

Information on the behavior of the entire film magnetization was obtained by making use of the magneto-optical Kerr effect (MOKE). In the longitudinal MOKE geometry, linearly polarized light is reflected off a magnetized sample. In order to record hysteresis loops, the change in the intensity of light that passes through an analyzing polarizer (set at an angle close to extinction) is monitored as the applied magnetic field is swept.[32] This intensity component is referred to as Kerr or MOKE intensity I_{MOKE}. The peak-to-peak intensity ΔI_{MOKE}, which is the difference in Kerr intensities, at positive and negative saturation magnetizations, is related to the amount of Kerr rotation and, in the case of thin films, to the total magnetic moment.[32,33] The Kerr signal can be expressed in percentage by using the ratio between ΔI_{MOKE} and the Kerr intensity I_{MOKE} at negative or positive saturation. Hysteresis loops were recorded for fields ranging from +200 to −200 Oe, which were generated by external Helmholtz coils. Sample temperatures down to 135 K were achieved by cooling the sample holder with liquid nitrogen.

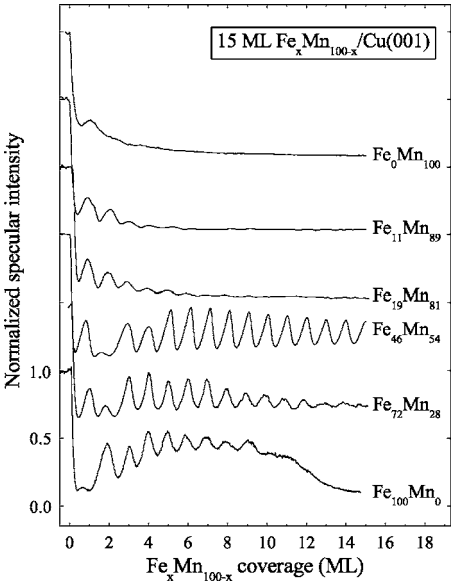

FIG. 1. Normalized intensity of reflected 25 keV He atoms with increasing simultaneous depositions of Fe and Mn on Cu(001) at room temperature for different individual deposition rates. The curves are shifted equidistantly with respect to the data for $Fe_{100}Mn_0$ at the bottom.

III. GROWTH, CHEMICAL COMPOSITION, AND CRYSTALLINE STRUCTURE

The specular He beam intensity has been recorded during simultaneous depositions of Mn and Fe at different individual rates (Fig. 1). The observed oscillatory behavior reflects periodic changes in surface morphology[34] and allows one to determine the film thickness t. An intensity maximum corresponds to a film with small roughness, i.e., in the simplest case, a completed surface layer. The growth behavior of Fe_xMn_{100-x} alloy films on Cu(001) can be divided into three regimes: Mn-rich, intermediate, and Fe-rich. Strongly damped oscillations are characteristic of the Mn-rich side. For $Fe_{19}Mn_{81}$, several maxima occur, but with rapidly decreasing amplitudes. For pure Mn (Fe_0Mn_{100}), only the

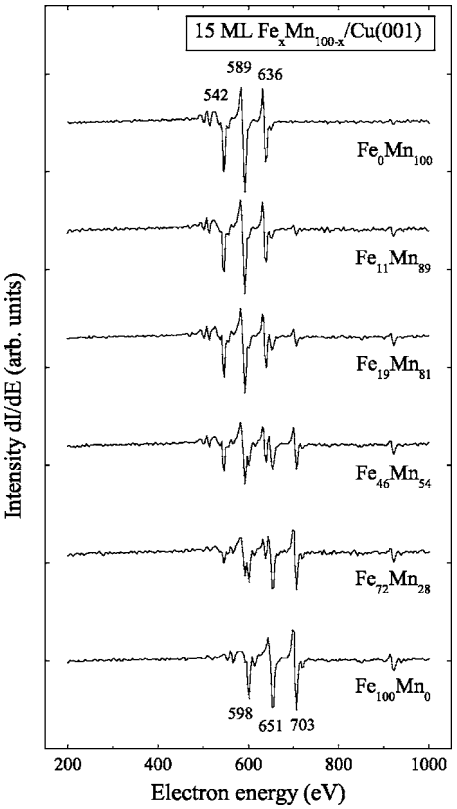

FIG. 2. Auger spectra of 15 ML Fe_xMn_{100-x} films with different alloy compositions.

maximum corresponding to the first monolayer can be identified. According to previous studies, a stable $Cu_{50}Mn_{50}$ surface alloy two layers thick is formed, after which Mn growth is rough.[35] For all Mn-rich films, the overall drop in intensity after a few monolayers is connected with a rough film surface.

In the intermediate range of alloy composition, equidistant oscillations are maintained up to coverages of more than 15 ML. In a range close to equal concentrations of Mn and Fe, the amplitudes only slightly decrease even for high coverages, indicating almost perfect layer-by-layer growth. A close inspection reveals the suppression of the maximum corresponding to the second monolayer, which is particularly pronounced for $Fe_{46}Mn_{54}$ in Fig. 1. The origin of this behavior is unclear, but may be connected with interface alloy formation in connection with the Cu(001) substrate at the initial stage of FeMn deposition.[15] The almost complete suppression of the second maximum in a very narrow concentration range provides additional experimental control over a specific alloy composition during film preparation.

On the Fe-rich side, growth oscillations occur up to about 10 ML. Above this coverage, the specular intensity decreases. In many studies, the sudden change in growth behavior has been identified by a structural transformation of the films from fcc-like to bcc-like.[17–19]

The overall behavior observed here by specular He beam scattering is similar to previous investigations on the growth of Fe_xMn_{100-x} films on Cu(001) using electron beam techniques such as medium energy electron diffraction[13] and reflection high energy electron diffraction.[15]

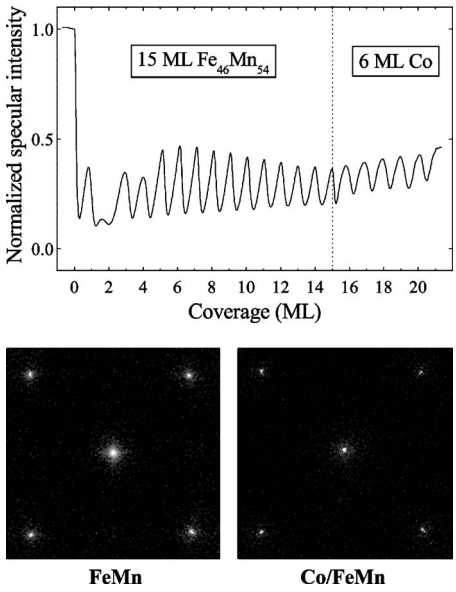

FIG. 3. Top: Normalized specular He beam intensity for the deposition of 6 ML Co/15 ML $Fe_{46}Mn_{54}$ bilayers. Bottom: Corresponding LEED pattern for the FeMn and the Co film (E_0 = 100 eV).

The characteristic growth behavior of the pure films (bottom and top of Fig. 1) provides the calibration of the Fe and Mn sources. Different alloy compositions are readily obtained by adjusting the individual deposition rates. The final quantitative determination of the chemical composition of the films (given at the right of Figs. 1 and 2) follows from Auger electron spectroscopy after deposition. The corresponding differential spectra dI/dE for the excitation by 4 keV primary electrons are shown in Fig. 2. The $L_3M_{23}M_{23}$, $L_3M_{23}M_{45}$, and $L_3M_{45}M_{45}$ Auger transitions of both elements extend over an energy range from 540 to 700 eV. Element-specific energies are given at the bottom (Fe) and at the top (Mn) of Fig. 2. The relative heights of the Fe and Mn signals systematically change with alloy composition. The Fe and Mn Auger signals are partly superimposed. Therefore, the relative amounts of Fe and Mn are obtained from the peak-to-peak heights of the Mn $L_3M_{23}M_{23}$ signal at 542 eV and the Fe $L_3M_{45}M_{45}$ signal at 703 eV. Different Auger electron cross sections for the corresponding Mn and Fe transitions are taken into account by reference data from literature[36] and the spectra of the pure films. The probing depth of the Fe and Mn LMM-Auger electrons amounts to approximately 5–7 ML (10–14 Å),[37] i.e., averaging over a substantial part of the total film. Alternatively, it is possible to determine the alloy composition from direct comparison of the Fe_xMn_{100-x} deposition rate by keeping the rate of Fe evaporation fixed.[13] In this case, the Mn fraction is given by the change in the time period of the growth oscillations.

Information on the crystalline structure of the Fe_xMn_{100-x} alloy films is obtained from LEED (Fig. 3). The diffraction spots appear at the same positions as the fcc(001) substrate spots. Additionally, IBT allows one to determine the atomic structure of the topmost surface layer in real space by making use of channeling phenomena during grazing ion scatter-

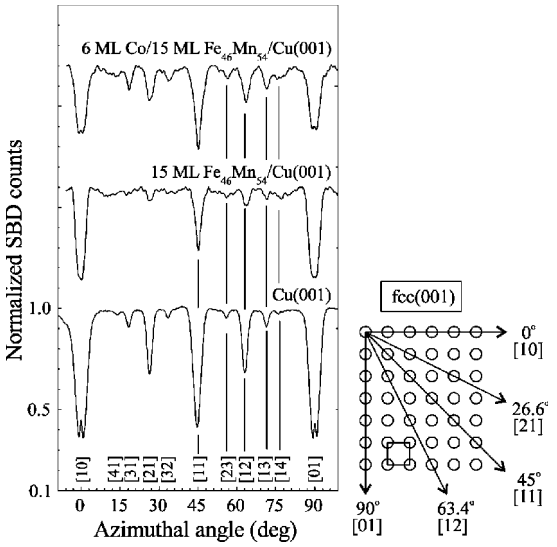

FIG. 4. Left: Normalized surface barrier detector counts versus azimuthal angle of incidence for grazing scattering of 29 keV protons ($\Phi_{in} \approx 1.6°$) at the surface of the Cu(001) crystal and different films. The IBT curves are shifted equidistantly with respect to the data at the bottom. Right: Schematic illustration of the fcc(001) surface and low-index directions.

ing (Fig. 4). For the clean fcc(001) surface of Cu, the IBT curve shows pronounced minima at low-index directions $[uv]$ in the primitive square surface lattice. The low-index directions and the angular settings with respect to the [10] direction are illustrated at the right of Fig. 4. For $Fe_{46}Mn_{54}/Cu(001)$, the absolute and relative sizes of the minima differ from Cu(001), but not the angular positions. It can, thus, be concluded that the surface of the films retains the initial in-plane substrate structure. LEED and IBT confirm that Fe_xMn_{100-x} alloy films close to equal concentration are pseudomorphic with respect to the Cu(001) crystal. This supports the established picture that γ-Fe_xMn_{100-x} is formed in the concentration regime II.[13,15]

The growth of Co on top of 15 ML $Fe_xMn_{100-x}/Cu(001)$ also proceeds layer by layer in regime II (top panel of Fig. 3). Compared to the Fe_xMn_{100-x} underlayer, the smoothness and the structure of the surface slightly improve with increasing Co deposition, which follows from a continuously increasing specular He beam intensity and a sharpening of the LEED spots. In addition, characteristic signatures in the IBT curve become more pronounced again (topmost curve in Fig. 4).

IV. THICKNESS AND TEMPERATURE DEPENDENT MAGNETIC PROPERTIES

The magnetic properties of Co/Fe_xMn_{100-x} bilayers with FeMn alloys close to equal concentrations (FeMn here denotes $x \approx 50$) have been studied by systematic variation of the FeMn layer thickness. For a 6 ML Co/4 ML FeMn bilayer, the coercivity of the MOKE hysteresis loop amounts to $H_C = 4$ Oe at a temperature of $T = 300$ K (top panel of Fig. 5), which is similar to the coercivity of the corresponding single

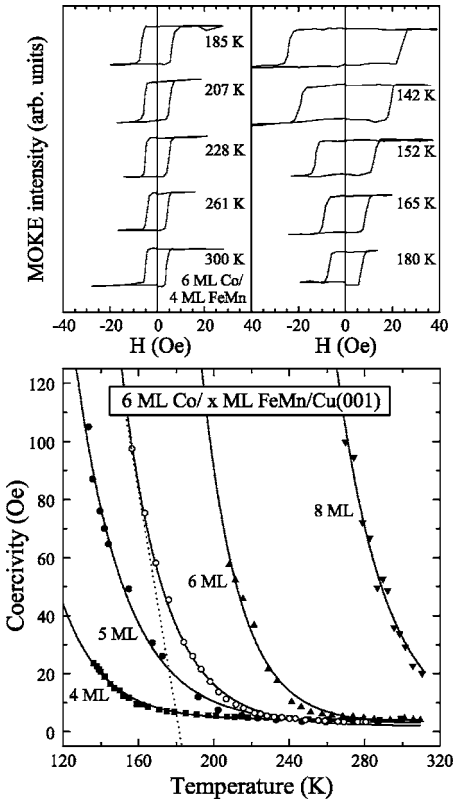

FIG. 5. Top: MOKE hysteresis loops with decreasing temperature from $T = 300$ K to $T = 135$ K for a 6 ML Co/4 ML FeMn bilayer. Bottom: Coercivity H_C as function of temperature for 6 ML Co/x ML FeMn bilayers with different FeMn thicknesses and alloys close to equal concentrations. Solid symbols, along ⟨100⟩ directions; open symbols, along ⟨110⟩ directions. Solid curves are guides for the eyes.

Co layer on Cu(001).[31] H_C significantly increases with decreasing temperature, while the hysteresis loops retain their almost rectangular shape within the measured temperature range. With increasing FeMn thickness, the onset of the H_C increase shifts to higher temperatures when keeping the Co thickness fixed (bottom panel of Fig. 5).

A striking phenomenon associated with the magnetic coupling at interfaces of FM and AFM materials is exchange bias, i.e., the shift H_E of the hysteresis loop from zero field. Other effects might be of the same magnitude or even larger. One is the increase in loop half-width H_C, which can be attributed to irreversible changes in the AFM spin structure during magnetization reversal of the exchange-coupled ferromagnet.[4] When the FM magnetization changes its direction, it may "drag" AFM spins, which increases the coercivity H_C. An additional AFM-induced anisotropy energy has to be overcome.

The induced coercivity H_C is large compared to the exchange bias H_E if the thickness of the AFM film is small, or if the temperature is close to the "blocking" temperature T_B,[4] where the exchange bias vanishes. In both cases, the total AFM anisotropy energy is relatively small and irreversible processes in the AFM film dominate the hysteresis loop behavior of the exchange-coupled ferromagnet. The H_E/H_C ra-

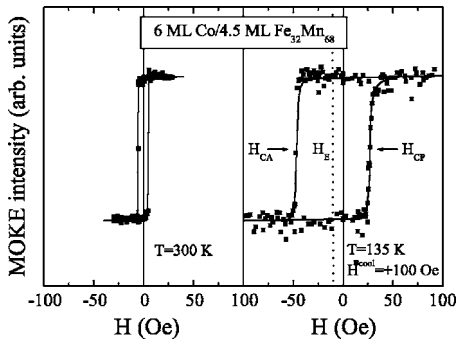

FIG. 6. MOKE hysteresis loops for a 6 ML Co/4.5 ML FeMn bilayer at $T=300$ K (left) and at $T=135$ K (right) after cooling in a positive field $H^{cool}=+100$ Oe.

tio provides a quantitative measure of this effect. For FM/AFM bilayers with $H_E/H_C \ll 1$, the term "exchange anisotropy" is appropriate rather than exchange bias. The FM/AFM exchange coupling leads to an appreciable loop broadening, but to a small loop shift. For MBE-grown Co/FeMn bilayers in the ultrathin film limit, exchange anisotropy is significant, but exchange bias is small. The increase in H_C with decreasing temperature is due to an increase in AFM anisotropy with decreasing temperature. Higher external fields are necessary to drag AFM spins during magnetization reversal at low temperature.

An example for exchange bias is shown in Fig. 6. After cooling in a positive field from $T=300$ K, the loop shift H_E amounts to -10 Oe at $T=135$ K for a 6 ML Co/4.5 ML FeMn bilayer. This corresponds to an exchange bias energy $\Delta E=H_E M_{FM} t_{FM}=0.0017$ erg/cm^2, which is 1–2 orders of magnitude smaller than in other FM/FeMn systems.[4,38,39]

Under the conditions described above, the coercivity becomes a measure of the magnetic anisotropy of the exchange-coupled FM/AFM system. For the investigated FeMn thicknesses up to 8 ML, H_C is larger along $\langle 110\rangle$ directions than along $\langle 100\rangle$ directions. The easy magnetization directions of the 6 ML Co/x ML FeMn bilayers are, thus, the same as for single Co layers on Cu(001), i.e., $\langle 110\rangle$ directions. In Fig. 5, H_C versus T is not shown for both easy and hard axes of magnetization in order to provide a clear presentation. The data for the hard axis of magnetization are mainly chosen because the properties of the bilayer with 8 ML FeMn thickness can be included in the temperature range up to 300 K.

For exchange-coupled FM/AFM bilayers, analytical expressions for the temperature dependence of the coercivity are rare[40] and not applicable to the MBE-grown Co/FeMn bilayers. Due to the complex magnetic and structural properties at the interface, numerical calculations are required to describe the AFM-induced coercivity increase in most of the theoretical models.[41–44] In many cases, an almost linear behavior or, more precisely, an almost linear falloff $\propto(1-T/T_B')$ is found over a wide temperature range,[42–44] with $T_B' \approx T_B$ and T_B being the blocking temperature of exchange bias.[4] Deviations from linearity exist close to the temperature where the FM/AFM coupling vanishes, which is usually given by the ordering temperature T_{AFM} of the AFM film. In a variety of experimental studies, a small peak or a nonlinear gradual decrease in H_C has been observed close to this temperature.[45–48] In random-field treatments of the interfacial coupling, the coercivity behavior in the transition region strongly depends on the interface roughness because it is crucial for the microscopic spin configuration in the antiferromagnet.[42]

With increasing temperature, the coercivity of Co/FeMn bilayers shows a gradually decaying tail immediately before a constant minimum value is reached (bottom panel of Fig. 5). Because a direct theoretical relationship between the coercivity behavior and T_{AFM} is not available, the ordering temperature is derived from the intercept of the tangent in the linear region with the temperature axis (dotted line in Fig. 5). The value T_{AFM}' thus obtained is a lower limit of the true ordering temperature T_{AFM}.

For 6 ML Co/5 ML FeMn bilayers, T_{AFM}' amounts to about 180 K. This is 40 K lower than the onset of the coercivity change, which is at about 220 K. The onset of the AFM-induced coercivity increase is assumed to be above the long-range ordering temperature T_{AFM} because AFM short-range interactions are likely to be sufficient to locally modify the reversal of the FM magnetization. T_{AFM}' shifts by 30–60 K per ML of FeMn.

We find that at room temperature, the AFM state is established for an FeMn thickness of 8 ML, which is 2 ML lower than reported in previous studies on MBE-grown Co/FeMn and FeMn/Co bilayers on Cu(001).[13,49] The reason for the discrepancy may be the fact that, in previous work, hysteresis loop measurements have mainly been performed in the case of FeMn/Co bilayers,[13] whereas the information on Co/FeMn bilayers has been obtained by magnetic domain imaging using photoemission electron emission microscopy.[49] The change in magnetic domain pattern is less accurate than the change in coercivity of the hysteresis loop. The previous conclusion[49] that FeMn layers in both Co/FeMn and FeMn/Co on Cu(001) become antiferromagnetic at room temperature at the same thickness of 10 ML seems to be incorrect. It has been found earlier that the value of T_{AFM} can vary due to the proximity of FM layers.[50]

Even for 4 ML FeMn, signatures of antiferromagnetic behavior are detected for temperatures between 160 and 135 K, the lowest temperature accessible in our experiments. It would be an interesting challenge to extend these investigations to even lower temperatures and smaller FeMn thicknesses in order to explore the limits of antiferromagnetism in binary metal alloys.

At room temperature, the AFM state is established for an FeMn thickness of 8 ML. A Kerr signal ΔI_{MOKE}, i.e., a difference in MOKE intensity for opposite magnetization directions, is not detected above this thickness because it is impossible to overcome the AFM-induced magnetic anisotropy energy of the ferromagnet. Then a complete hysteresis loop cannot be recorded because our maximum accessible field of $H=\pm 200$ Oe is not sufficient for magnetization reversal. This is valid not only for Fe_xMn_{100-x} alloys with equal concentrations, but rather for an extended concentration range: $20-30 \leqslant x \leqslant 50-60$ (solid squares in Fig. 7). On the Mn-rich (Fe-rich) side, the Kerr signal continuously increases with decreasing (increasing) Fe content. The normalized Kerr sig-

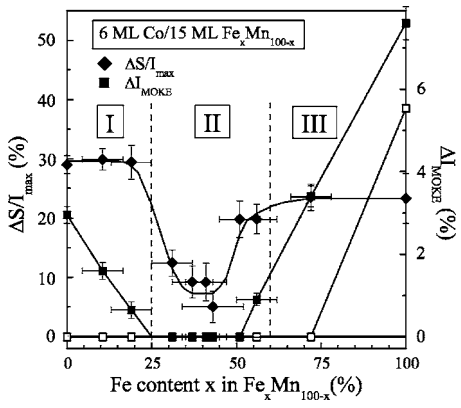

FIG. 7. Kerr signal ΔI_{MOKE} for 6 ML Co/15 ML Fe_xMn_{100-x} bilayers (solid squares) and 15 ML Fe_xMn_{100-x} single layers (open squares) with different alloy compositions (right scale). Corresponding $\Delta S/I_{max}$ obtained from hysteresis loops recorded by electron capture, only for the bilayers (left scale). All data refer to $T=300$ K. Solid lines are guides for the eyes.

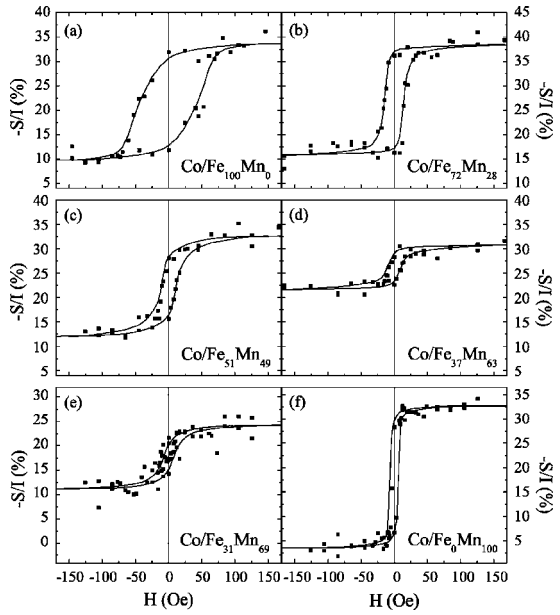

FIG. 8. EC hysteresis loops for 6 ML Co/15 ML Fe_xMn_{100-x} bilayers with different alloy compositions at $T=300$ K. The scale ranges of the ordinate axes are the same. Solid lines are guides for the eyes.

nal ΔI_{MOKE} of a single 6 ML Co film of about 3% is reached at $x=0$ on the Mn-rich side and at $x\approx 70-75$ on the Fe-rich side. In ultrathin ferromagnetic films of Fe, Co, and Ni, the Kerr signal is proportional to the thickness, which determines the total magnetic moment.[51] It can, thus, be concluded that the full Kerr signal due to a reversal of the entire Co magnetization only occurs for $x=0$ and $x\geqslant 50-60$. For other Fe_xMn_{100-x} alloy compositions, a partial or a complete pinning of the Co magnetization by the Fe_xMn_{100-x} exists, which is explained by the interface coupling between the ferromagnetic Co and the antiferromagnetic Fe_xMn_{100-x}.

The behavior determined by MOKE for 6 ML Co/15 ML Fe_xMn_{100-x} bilayers with different alloy compositions can be summarized as follows:

(I) $0<x\leqslant 20-30$: partial Co pinning and AFM FeMn ordering;

(II) $20-30\leqslant x\leqslant 50-60$: strong Co pinning and AFM FeMn ordering;

(III) $x\geqslant 60-70$: no Co pinning and paramagnetic to ferromagnetic FeMn ordering.

This classification is similar to the three concentration regimes for bulk Fe_xMn_{100-x} alloys mentioned in the Introduction. It is also supported by experiments on EC, which probe the surface magnetization compared to the complete film magnetization like MOKE.

Under certain conditions, EC hysteresis loops provide information on the fractions of reversed and pinned magnetizations of the surface. Differences in the magnetization reversal averaged over the whole film volume and the magnetization reversal averaged over the topmost surface layer can, thus, be detected by a comparison of MOKE and EC hysteresis loops, i.e., from the change in the MOKE and EC signals in opposite external fields. Differences are expected to occur due to noncollinearities of surface and bulk magnetizations, or due to the formation of partial domain walls within the FM film parallel to the surface. The latter is discussed in more detail below.

EC hysteresis loops are obtained by monitoring the Stokes parameter S/I as a function of external field (Fig. 8). Different from MOKE, hysteresis loops can be detected over the entire concentration range but with varying shapes. For 6 ML Co/15 ML $Fe_{100}Mn_0$ and 6 ML Co/15 ML Fe_0Mn_{100} bilayers, the hysteresis loops are similar to the corresponding MOKE data. In the first case, the coercivity is relatively large due to strong exchange coupling between the Co layer and the underlying Fe layer, which possesses a coercivity of about 50–100 Oe on Cu(001).[52] In the second case, the hysteresis loop is almost the same as for a 6 ML Co single layer because pure Mn has a negligible magnetic effect, indicating paramagnetism in this thickness range.

The reversible part of the surface magnetization is related to the normalized parameter $\Delta S/I$; here, $\Delta S/I_{max}=S/I(H=+200\ \text{Oe})-S/I(H=-200\ \text{Oe})$. It corresponds to the Kerr signal ΔI_{MOKE} of the entire film magnetization. For the 6 ML Co/15 ML $Fe_{100}Mn_0$ and the 6 ML Co/15 ML Fe_0Mn_{100} bilayers, $\Delta S/I_{max}$ amounts to about 25%–30%, which is similar to the value for 6 ML Co because the magnetization of the entire film and the surface is reversed during the field sweep. The same holds for bilayers containing an Fe-rich alloy like $Fe_{72}Mn_{28}$ in Fig. 8(b). The corresponding spin polarization of the captured Co electrons is $P_s\approx 17\%-20\%$.[31]

In the intermediate concentration range, $\Delta S/I_{max}$ decreases [Figs. 8(c)–8(e)] as illustrated by the solid diamonds in Fig. 7. Because $\Delta S/I$ is a measure of the surface magnetization,[30,31] the reduction in $\Delta S/I$ is due to an incomplete magnetization reversal. One part is moved by the external magnetic field, while another part is pinned as a result of the strong Co/Fe_xMn_{100-x} coupling. The fraction of reversed surface magnetization is smallest for the intermediate concentration regime $(20-30\leqslant x\leqslant 50-60)$. The difference in the data obtained by EC and MOKE is attributed to the probing depths.

The spin polarization and the magnetization of the topmost atomic layer at the surface are probed by electron capture ($\lambda \rightarrow 0$ ML). The MOKE signal provides information on the entire magnetization of a thin film including both interfaces. Even in the case of a film of 6 ML (12 Å) thickness, the signal is predominantly due to the interior of the film. It is, thus, adequate to consider a "bulk" magnetization probed by MOKE as opposed to a surface magnetization probed by EC. Recent experimental studies on thin ferromagnetic films with thicknesses of about ten of to several tens of angstroms confirm significant differences in the orientation of the interface and bulk magnetizations during reversal in an external field. These findings have either been attributed to weakened exchange interactions at the interface[31,53] or to interface-induced anisotropies.[54] If a FM layer is exchange coupled to an AFM layer, differences in the direction of the surface, interface, and bulk magnetizations can occur due to the AFM-induced anisotropy at the FM/AFM interface. During magnetization reversal, a partial domain wall or a spin spiral may develop in the ferromagnet, with spin rotations parallel to the interface.[55,56] The degree of rotation depends on the thickness of the ferromagnetic film. In ultrathin films, it is expected to be small but detectable by comparison of MOKE and EC measurements.[31] The intention of the comparison of MOKE and EC hysteresis loops is the detection of noncollinearities between surface and bulk magnetizations during magnetization reversal, which provides indirect information on the nature of the FM/AFM coupling mechanism.

For the Co/Fe_xMn_{100-x} bilayers, the difference in reversible magnetization at the surface and the bulk has a maximum for alloy compositions of $x \approx 50$ (Fig. 7). For $20-30 \leqslant x \leqslant 50-60$, the bulk magnetization is fixed, while minor hysteresis loops are still detected for the surface magnetization. The concentration dependence of $\Delta S/I_{max}$ is in line with the classification into three regimes.

The difference in surface and bulk magnetizations is attributed to changes in exchange interaction or magnetic anisotropy due to reduced site symmetry and coordination at the surface. Magnetic moments at surface terrace edges and surface defects play a decisive role because noncollinearities between spins in the surface and the bulk exist during magnetization reversal. These spins may be considered as "loose spins" with weakened exchange interaction. The existence of the latter has been postulated in the field of exchange coupling in ferromagnetic/nonmagnetic multilayers under certain conditions.[57] Spin rotations in the interior of the Co film seem to exist on the Mn-rich side of the Fe_xMn_{100-x} alloys, but not in the intermediate region close to equal concentrations. However, there exists no preferred pinning of the magnetization at the Co surface as opposed to the Co/FeMn interface.

An alternative explanation for the difference in surface and bulk magnetizations is a difference in ordering temperature T_C of the surface and the bulk of the FM film. If the sample temperature is not sufficiently below the surface ordering temperature, the surface magnetization may adjust much easier to external fields. In the case of a 6 ML Co film, this behavior can be discarded because a Co film of 2 ML already possesses an ordering temperature appreciably above room temperature as evidenced by recent EC measurements.[58] The FM ordering temperature for 6 ML Co/15 ML FeMn is far above room temperature. In this regard, Co/FeMn bilayers are comparable to Co single layers on Cu(001). For 3 ML Co on Cu(001), T_C amounts to almost 600 K.[59]

V. SUMMARY

The magnetic properties of Co/Fe_xMn_{100-x} bilayers in the ultrathin film limit with total thicknesses below 20–25 ML strongly depend on alloy composition and thickness. Changes in the hysteresis loop behavior are explained by magnetic interface coupling due to antiferromagnetic ordering in the Fe_xMn_{100-x} alloys. The concentration dependence of the magnetic properties provides a classification into three regimes. The strongest coupling effects are found in the intermediate regime ($20-30 \leqslant x \leqslant 50-60$), which corresponds to the existence of bulk γ-Fe_xMn_{100-x}.

We find that at room temperature, the antiferromagnetic state is established for an $Fe_{50}Mn_{50}$ thickness as small as 8 ML. Down to a thickness of 4 ML FeMn, signatures of antiferromagnetic behavior are detected for temperatures between 160 and 135 K. This experimental result is a challenge for future investigations at lower temperatures and smaller FeMn thicknesses, which should elucidate the limits under which antiferromagnetism in binary metal alloys is established.

For 15 ML Fe_xMn_{100-x}, we find a different behavior of surface and bulk magnetization reversal for the Co films at room temperature. For the intermediate concentration regime ($20-30 \leqslant x \leqslant 50-60$), the fraction of reversed surface magnetization is smallest, which corresponds to the strongest Co/Fe_xMn_{100-x} coupling. The difference in reversal behavior of surface and bulk magnetizations may originate from weakened exchange interactions at the surface and from defects.

ACKNOWLEDGMENTS

We thank K. Maass and G. Lindenberg for their assistance in the preparation of the experiments. This work was supported by the Deutsche Forschungsgemeinschaft (Wi 1336).

*Corresponding author; markus.gruyters@gmx.de

[1] A. Moser, K. Takano, D. T. Margulies, M. Albrecht, Y. Sonobe, Y. Ikeda, S. Sun, and E. E. Fullerton, J. Phys. D **35**, R157 (2002).
[2] W. J. Gallagher and S. S. P. Parkin, IBM J. Res. Dev. **50**, 5 (2006).
[3] P. Grünberg, Phys. Today **54** (5), 31 (2001).
[4] J. Nogués and I. K. Schuller, J. Magn. Magn. Mater. **192**, 203 (1999).

[5] H. Umebayashi and Y. Ishikawa, J. Phys. Soc. Jpn. **21**, 1281 (1966).
[6] Y. Endoh and Y. Ishikawa, J. Phys. Soc. Jpn. **30**, 1614 (1971).
[7] *3d, 4d and 5d Elements, Alloys and Compounds*, edited by H. P. J. Wijn, Landolt Börnstein, New Series, Group III, Vol. 19, Pt. A (Springer-Verlag, Berlin, 1986).
[8] A. Déchelette, J. M. Tonnerre, M. C. Saint Lager, F. Bartolomé, L. Sève, D. Raoux, H. Fischer, M. Piecuch, V. Chakarian, and C. C. Kao, Phys. Rev. B **60**, 6636 (1999).
[9] C. Tsang, N. Heiman, and K. Lee, J. Appl. Phys. **52**, 2471 (1981).
[10] W. J. Antel, F. Perjeru, and G. R. Harp, Phys. Rev. Lett. **83**, 1439 (1999).
[11] V. I. Nikitenko, V. S. Gornakov, A. J. Shapiro, R. D. Shull, K. Liu, S. M. Zhou, and C. L. Chien, Phys. Rev. Lett. **84**, 765 (2000).
[12] F. Y. Yang and C. L. Chien, Phys. Rev. Lett. **85**, 2597 (2000).
[13] F. Offi, W. Kuch, and J. Kirschner, Phys. Rev. B **66**, 064419 (2002).
[14] F. Offi, W. Kuch, L. I. Chelaru, K. Fukumoto, M. Kotsugi, and J. Kirschner, Phys. Rev. B **67**, 094419 (2003).
[15] R. Thamankar, S. Bhagwat, and F. O. Schumann, Phys. Rev. B **69**, 054411 (2004).
[16] C. Won, Y. Z. Wu, H. W. Zhao, A. Scholl, A. Doran, W. Kim, T. L. Owens, X. F. Jin, and Z. Q. Qiu, Phys. Rev. B **71**, 024406 (2005).
[17] J. Thomassen, F. May, B. Feldmann, M. Wuttig, and H. Ibach, Phys. Rev. Lett. **69**, 3831 (1992).
[18] J. Shen and J. Kirschner, Surf. Sci. **500**, 300 (2002).
[19] T. Bernhard, M. Baron, M. Gruyters, and H. Winter, Phys. Rev. Lett. **95**, 087601 (2005).
[20] H. Li and B. P. Tonner, Surf. Sci. **237**, 141 (1990).
[21] J. Fassbender, U. May, B. Schirmer, R. M. Jungblut, B. Hillebrands, and G. Güntherodt, Phys. Rev. Lett. **75**, 4476 (1995).
[22] R. Pfandzelter, T. Bernhard, and H. Winter, Phys. Rev. Lett. **90**, 036102 (2003).
[23] H. Winter, K. Maass, S. Lederer, HP. Winter, and F. Aumayr, Phys. Rev. B **69**, 054110 (2004).
[24] F. Aumayr, G. Lakits, and H. P. Winter, Appl. Surf. Sci. **47**, 139 (1991).
[25] M. Baron, T. Bernhard, M. Gruyters, and H. Winter, Surf. Sci. **600**, 3924 (2006).
[26] H. Winter, H. Hagedorn, R. Zimny, H. Nienhaus, and J. Kirschner, Phys. Rev. Lett. **62**, 296 (1989).
[27] H. Winter, Z. Phys. D: At., Mol. Clusters **23**, 41 (1992).
[28] J. Leuker, H. W. Ortjohann, R. Zimny, and H. Winter, Surf. Sci. **388**, 262 (1997).
[29] R. Guenther, *Modern Optics* (Wiley, New York, 1990).
[30] R. Pfandzelter and M. Potthoff, Phys. Rev. B **64**, 140405(R) (2001).
[31] M. Gruyters, T. Bernhard, and H. Winter, Phys. Rev. Lett. **94**, 227205 (2005).
[32] C. Liu, E. R. Moog, and S. D. Bader, Phys. Rev. Lett. **60**, 2422 (1988).
[33] E. Mentz, A. Bauer, T. Günther, and G. Kaindl, Phys. Rev. B **60**, 7379 (1999).
[34] M. H. Langelaar and D. O. Boerma, Surf. Sci. **436**, 237 (1999).
[35] T. Flores, M. Hansen, and M. Wuttig, Surf. Sci. **279**, 251 (1992).
[36] L. E. Davis, N. C. MacDonald, P. W. Palmberg, G. E. Riach, and R. E. Weber, *Handbook of Auger Electron Spectroscopy* (Perkin-Elmer Corporation, Eden Prairie, 1978).
[37] M. P. Seah and W. A. Dench, Surf. Interface Anal. **1**, 2 (1979).
[38] R. M. Jungblut, R. Coehoorn, M. T. Johnson, J. aan de Stegge, and A. Reinders, J. Appl. Phys. **75**, 6659 (1994).
[39] M. Ali, C. H. Marrows, and B. J. Hickey, Phys. Rev. B **67**, 172405 (2003).
[40] G. Scholten, K. D. Usadel, and U. Nowak, Phys. Rev. B **71**, 064413 (2005).
[41] M. D. Stiles and R. D. McMichael, Phys. Rev. B **63**, 064405 (2001).
[42] J. R. L. de Almeida and S. M. Rezende, Phys. Rev. B **65**, 092412 (2002).
[43] Z. Huang, S. Li, H. Lin, F. Zhang, and Y. Du, J. Magn. Magn. Mater. **303**, e180 (2006).
[44] Z. Nishioka, S. Hou, H. Fujiwara, and R. D. Metzger, J. Appl. Phys. **80**, 4528 (1996).
[45] X. W. Wu and C. L. Chien, Phys. Rev. Lett. **81**, 2795 (1998).
[46] C. Leighton, M. Song, J. Nogués, M. C. Cyrille, and I. K. Schuller, J. Appl. Phys. **88**, 344 (2000).
[47] I. N. Krivorotov, T. Gredig, K. R. Nikolaev, A. M. Goldman, and E. D. Dahlberg, Phys. Rev. B **65**, 180406(R) (2002).
[48] F. Radu, M. Etzkorn, R. Siebrecht, T. Schmitte, K. Westerholt, and H. Zabel, Phys. Rev. B **67**, 134409 (2003).
[49] W. Kuch, F. Offi, L. I. Chelaru, M. Kotsugi, K. Fukumoto, and J. Kirschner, Phys. Rev. B **65**, 140408(R) (2002).
[50] P. J. van der Zaag, Y. Ijiri, J. A. Borchers, L. F. Feiner, R. M. Wolf, J. M. Gaines, R. W. Erwin, and M. A. Verheijen, Phys. Rev. Lett. **84**, 6102 (2000).
[51] Z. Q. Qiu, J. Pearson, and S. D. Bader, Phys. Rev. B **45**, 7211 (1992).
[52] T. Bernhard, M. Baron, M. Gruyters, and H. Winter, Surf. Sci. **600**, 1877 (2006).
[53] L. Péter, Z. Rolik, L. F. Kiss, J. Tóth, V. Weihnacht, C. M. Schneider, and I. Bakonyi, Phys. Rev. B **73**, 174410 (2006).
[54] H. B. Zhao, D. Talbayev, G. Lüpke, A. T. Hanbicki, C. H. Li, M. J. van't Erve, G. Kioseoglou, and B. T. Jonker, Phys. Rev. Lett. **95**, 137202 (2005).
[55] M. Kiwi, J. Magn. Magn. Mater. **234**, 584 (2001).
[56] R. L. Stamps, J. Phys. D **33**, R247 (2000).
[57] J. C. Slonczewski, J. Appl. Phys. **73**, 5957 (1993).
[58] M. Gruyters, T. Bernhard, and H. Winter, J. Magn. Magn. Mater. **292**, 192 (2005).
[59] C. M. Schneider, P. Bressler, P. Schuster, J. Kirschner, J. J. de Miguel, and R. Miranda, Phys. Rev. Lett. **64**, 1059 (1990).